An MRI compatible loading device for the reconstruction of clinically relevant plantar pressure distributions and loading scenarios of the forefoot

Panagiotis E. Chatzistergos[(1),(*)], Roozbeh Naemi[(1)], Nachiappan Chockalingam[(1)]

(1)   CSHER, Faculty of Health Sciences, Staffordshire University, Stoke-on-Trent, United Kingdom.

(*)   Corresponding author,   **tel.:** +44 1782 295920

       e-mail: panagiotis.chatzistergos@staffs.ac.uk

28   **Abstract:**

29   This study aims to present a new MRI compatible loading device capable of reconstructing realistic

30   loading scenarios of the human foot for research in the field of foot biomechanics. This device has

31   two different configurations: one used to compress the forefoot and one to bend the

32   metatarsophalangeal joints. Required plantar pressure distribution under the metatarsal heads can be

33   achieved by modifying the distribution of the dorsally applied forces. To validate the device, subject-

34   specific plantar pressures were measured and then reconstructed using the device. For quiet stance the

35   peak pressure reconstruction error was 3% while for mid-stance phase of gait it was 8%. The device

36   was also used to measure the passive bending stiffness of the metatarsophalangeal joints of one

37   subject with low intra-subject variability. A series of preliminary MRI scans confirmed that the

38   loading device can be used to produce static weight-bearing images of the foot (voxel size:

39   0.23mm×0.23mm×1.00mm).

40

41   The results indicate that the device presented here can accurately reconstruct subject specific plantar

42   pressure distributions and measure the foot's metatarsophalangeal passive stiffness. Possible future

43   applications include the validation of finite element models, the investigation of the relationship

44   between plantar pressure and internal stresses/strains and the study of the foot's inter-segmental

45   passive stiffness.

46

47

48

49

50

51

52

53

54

55

1.   Introduction

Investigating the internal stresses and strains of the human foot soft tissues is crucial to the understanding of foot biomechanics [1,2]. The significance of internal tissue stress and strain is even more pronounced in the case of the diabetic foot. Previous research indicates that ulceration begins internally and could be caused by deep tissue trauma [3]. In this context a number of different methodologies have been developed for the direct measurement of internal strains using medical imaging [2,4–12]. These protocols usually involve a comparison of an unloaded image of the tissue's structure against the images of the loaded structures under a range of externally applied loads. The implementation of this concept requires a method with three main constituents: a medical imaging modality, a tissue-loading device and an algorithm/procedure to quantify and map the changes of the tissues' structure [10].

From the common imaging modalities Magnetic Resonance Imaging (MRI) appears to be the most suited one for a detailed analysis of the three dimensional (3D) field of internal deformations of soft tissues [2]. MRI offers a superb contrast for the imaging of soft tissues and it doesn't employ any ionizing radiation. However, one of the main disadvantages of using MRI is the fact that applying loads in a controlled and repeatable manner inside an MRI scanner is considerably more difficult compared to other available modalities such us ultrasonography [4], fluoroscopy [5,6] or computer tomography (CT) [7–9]. The use of MRI imposes a number of limitations in terms of the dimensions and the materials that can be used to build a loading device, hence a number of studies have looked at tackling this challenge for various anatomical regions [2,13].

To investigate the internal deformations of the foot, Petre et al. [2] developed a sophisticated MRI compatible loading device capable of applying both normal and shear loads to the forefoot. The pilottesting of this device indicated that despite its capacity to apply "gait-like loading" [2] it couldn't generate plantar pressure distributions similar to the ones measured during walking. This was attributed to the fact that the loading device simultaneously applied a net force to both the metatarsal head (MTH) and toe regions and there was no control over the distribution of the load [2].

3

84

85   In contrast to internal deformations, the internal stresses of plantar soft tissues cannot be directly

86   measured, but they can be estimated with the use of finite element (FE) models [1,10]. An accurate

87   3D FE model of the foot though, requires a large amount of information on its internal structure and

88   the mechanical properties of its soft tissues (i.e. skin, fat, muscle etc.). Furthermore to accurately

89   replicate realistic loading scenarios such models need information on the function and stiffness of its

90   numerous joints and they have to be validated against experimental data.

91

92   The bending stiffness of joints in general can be analysed in two components: a dynamic one

93   associated with active muscle forces and a passive one associated with the elastic properties of non-

94   contractile tissues [14]. Hence measuring the passive stiffness of the joints of the foot in addition to

95   enhancing our understanding on their function it can also give clinically relevant information about

96   the mechanical status of non-contractile tissues, such as ligaments, tendons etc.

97

98   In this context the present study aims to present a novel MRI compatible device for the accurate

99   reconstruction of subject specific plantar pressure distributions of the forefoot and the simulation of

100   clinically relevant loading scenarios. This device was designed and built to enable the study of the in-

101   vivo mechanical behaviour of the plantar soft tissues of the forefoot under compression as well as for

102   the study the mechanical behaviour of the passive foot under bending.

103

104   **2.   Participants and methods**

105   A total of six healthy volunteers (4 female, 2 male) with an average age of 33.0 (±6.3) years and

106   average body mass of 70.9 (±7.7) kg were recruited for this study (Table 1). Ethical approval was

107   sought and granted by the University Ethics Committee and the volunteers provided full informed

108   consent.

109

110   The MRI compatible loading device was designed using SolidWorks® 2010 (Dassault Systèmes, Paris,

111   France). The device consisted of custom made parts milled from polypropylene blocks and connected

112 with Nylon plastic screws and bolts. The device (Figure 1) has a fixed part (A) for foot support and a

113 movable one (B) for loading. The movable part (B) can rotate around a predefined axis (C). The

114 device can be configured so that the initial angle between part B and the plantar surface of part A is

115 either 90° or 0°. Each one of these two configurations enables the application of different load

116 scenarios (compression or bending modes respectively). In both cases the loading is applied with the

117 help of a suspended MRI compatible mass. The suspended mass can be up to 5 Kg which generates a

118 maximum compressive force of ≈250 N or bending moment of ≈7 Nm. During the design of the

119 loading device special attention was paid to minimize its dimensions and make sure it will fit inside a

120 typical MRI scanner with a bore aperture of 60 cm [15].

121

122 **2.1   Compression mode**

123 The loading device is capable of applying known compressive forces at the dorsal side of the forefoot.

124 For this purpose the movable part B (Figure 1A) is positioned at 90° with respect to the foot-support

125 (A) and equipped with a compression punch (D). This punch is used to compress the forefoot and to

126 control the distribution of the applied load. More specifically a series of screws is used to modify the

127 profile of the contact area between the punch and the dorsal surface of the foot (Figure 1A). The

128 relative position of the foot and punch can also be modified with the use of 5 mm thick plastic sheets

129 (E). Positioning the compression punch at the dorsal side of the MTHs enables the controlled loading

130 of the soft tissues that lie directly below them. When a compressive load is applied at the dorsal side

131 of the forefoot these non-contractile soft tissues (mainly skin and fat) are compressed between the

132 foot-support (A) and the MTHs.

133

134 The ability of this device to reconstruct subject specific plantar pressure distributions was assessed in

135 a pilot study. More specifically the loading device was used to reconstruct the plantar pressure

136 developed at the MTH region during quiet stance and the mid-stance phase of walking gait.

137

138 The quality of the MRI images that can be recorded when the foot is under the static weight bearing

139 conditions generated by the device was assessed in a series of preliminary scanning sequences. The

140 forefoot region of a volunteer was compressed with a net force of 250 N and imaged using a 1.5 T

141 MRI scanner. The duration of the scanning process was ≈ 4 min and coronal T1 weighted 3D Fast

142 Field Echo (FFE) images (Figure 2) were recorded with in-plane and out of plane resolution of 0.23

143 mm and 1.00 mm respectively. No plantar pressure measurement was performed inside the MRI

144 scanner.

145

146 **2.1.1   Quiet stance**

147   In the case of quiet stance the average peak pressure under each Metatarsal Head (MTH) was

148 measured for each of the six volunteers using a plantar pressure sensor (F-scan®, Tekscan, Boston,

149 MA, US) (Figure 1A). The volunteers stood on the sensor and the area under each MTH was

150 identified by applying pressure manually at the dorsal side of the foot. The relative location of each

151 MTH on the pressure sensor was utilized to measure the peak plantar pressure of each MTH (Figure

152 3). The plantar pressure was recorded at a sampling rate of 100 Hz for 10 sec of quiet stance and the

153 average peak pressure for each MTH was calculated to produce the reference measurements for the

154 reconstruction. The relative position of the foot and the sensor was fixed using double sided tape. The

155 volunteers' feet were then placed inside the loading device and a pressure was applied at the dorsal

156 side of their forefoot. The suspended mass was gradually increased (in increments of 0.5 Kg) to

157 approximate the total forefoot force. The profile of the punch was sequentially modified starting from

158 the MTH with the maximum reference pressure and then moving medially and laterally to reconstruct

159 the pattern of the reference plantar pressure distribution. This procedure was repeated until the

160 difference between the reference and the reconstructed peak pressures was less than 5%. After

161 achieving a satisfactory replication of the overall pattern of pressure distribution, the plantar pressure

162 was recorded again for 10 seconds at a sampling rate of 100 Hz. One additional pressure measurement

163 was performed for a single participant (participant #6) with the compression punch completely flat

164 (i.e. before any modification of its profile) to highlight the versatility of the loading device.

165

166 The duration of loading was decided based on preliminary results indicating that the plantar pressure

167 distribution generated by the loading device stays practically constant for long periods of time. More

6

168 specifically a net compressive force of 150 N was applied to the forefoot of a volunteer and the peak

169 plantar pressure was recorded at 1 Hz for 20 minutes of continuous loading. The average value and

170 standard deviation of the peak pressure was calculated.

171

172 The reproducibility of the results was assessed through a test re-test procedure (Table 1). After

173 completing all tests, the loading procedure and pressure measurements were repeated for one

174 volunteer (#5) without reconfiguring the loading device (i.e. the suspended mass and the profile of the

175 compression punch was the same for both test and re-test).

176

177 2.1.2   Mid-stance phase of gait

178 In the case of the mid-stance phase of gait the plantar pressure of a complete gait cycle was recorded

179 for a single volunteer (#5) using a walkway pressure mapping system (Walkway®, Tekscan, Boston,

180 MA, US). An automated procedure within the Walkway® system was used to identify the area below

181 each MTH and to measure the corresponding pressure in each region. In this case the reference values

182 for the reconstruction procedure were the peak pressures under the MTHs for a randomly selected

183 instance of the mid-stance phase of gait (50% of mid-stance). The plantar pressure developed inside

184 the loading device was measured again using F-scan®.

185

186 2.2   Bending mode

187 Reconfiguring the loading device allows the application of known bending moments to the foot. For

188 this purpose parts A and B are positioned parallel to one another and the compression punch is

189 removed (Figure 1B). In this configuration a rotation of part B around its axis (C) tends to bend the

190 subject's foot instead of compressing it. The relative position of the foot with respect to the rotation

191 axis can be modified with the use of 5 mm thick plastic sheets (E) (Figure 1B). These sheets are

192 placed between the foot and the foot's support elevating the foot along two axes: one parallel and one

193 perpendicular to the plantar surface (Figure 1B). When the device is used inside an MRI scanner the

194 relative angle between parts A and B can be measured from the MRI images.

195

196   The bending mode of the MRI compatible loading device was pilot tested for a single volunteer by

197   measuring the bending stiffness of the metatarsophalangeal (MP) joints. For this purpose the bending

198   axis of the volunteer's MP joints was first identified based on anatomical landmarks [16]. The

199   volunteer's foot was fixed inside the device using Velcro straps (Figure 1B) and using a goniometer

200   the bending angle of the MP joints was measured for bending moments ranging from 1.8 Nm to 4.5

201   Nm. Ten preconditioning load/unload cycles were performed before each measurement and each

202   measurement was repeated five times.

203

204   **3.   Results**

205   **3.1   Compression mode**

206   The pilot MRI scan indicated that the quality of the MRI images recorded when the foot is under the

207   static weight bearing conditions generated by the device have a resolution that is high enough to

208   enable the identification and segmentation of different tissues of the foot (Figure 2).

209

210   **3.1.1   Quiet stance**

211   In the case of quiet stance the average difference between the reference and the reconstructed total

212   maximum pressures was only 4% while the mean difference for all MTHs ranged between 2% and

213   15% (Table 1). In all cases the total maximum pressure was observed under the same MTH for both

214   the reconstructed and the reference pressure distributions. As it can be seen in Table 1 and Figure 3

215   the loading device was capable of reconstructing different and distinctive subject specific loading

216   patterns. The ability of the device to modify the distribution of plantar pressures becomes clearer if

217   one compares the initial pressures that are measured in the device before any adjustment of the

218   compression profile (i.e. for a compression profile that is completely flat) to the final ones after all

219   necessary adjustments had been completed (Figure 3).

220

221   Moreover the loading device was capable of maintaining a constant distribution of plantar pressure for

222   long periods of time. The average peak pressure measured for 20 minutes of continuous loading was

223   equal to 111.8 kPa with a standard deviation of only 4.3 kPa (i.e. 3.8% error). In terms of

8

224　reproducibility, the test-retest procedure yielded differences in terms of average peak pressures that

225　were lower than 5% (Table 1).

226

227　**3.1.2　Mid-stance phase of gait**

228　In the case of mid-stance phase of gait the average difference between the reference peak pressures

229　and the reconstructed average peak pressures was 8% (Table 1). The difference between the overall

230　maximum values was also 8%.

231

232　**3.2　Bending mode**

233　The standard deviation of the measured rotation angles for different values of the externally applied

234　moment was always lower than 3 deg indicating a relatively low intra-subject variability (Table 2).

235　Moreover, bending angle appeared to increase linearly with moment (R^2=0.98). The slope of the

236　moment/angle graph was equal to 0.06 Nm/deg.

237

238　**4.　Discussion**

239　The purpose of this study was to present a new foot loading device that is capable of reconstructing

240　clinically relevant loading scenarios inside an MRI scanner. This device was initially designed to

241　enable the validation of 3D FE models of the foot and more specifically to help assess their accuracy

242　to predict the internal stresses and strains of plantar soft tissues and to simulate the function of the

243　foot's joints. For this reason a custom made device was designed to allow two different configurations

244　for the application of different loads, i.e. compression and bending. Having two different

245　configurations for compression and bending enabled the realisation of different loading scenarios

246　using a single device instead of two while at the same time helped simplifying the design of the

247　device.

248

249　The new method for the reconstruction of subject specific pressure distributions presented here was

250　focused on the MTH area. The MTH area along with the heel and the hallux are the areas with the

251　highest ulceration rates in people with diabetes. A recent study by Ledoux et al. [17] demonstrated for

9

252   the first time that the ulceration risk for the MTH area is correlated to in-shoe peak plantar pressure.

253   No similar correlation was found for the heel and hallux which could indicate that in the case of the

254   MTH area ulceration is caused by normal loading instead of shear while in the case of the heel and

255   hallux shear loading (among other reasons) could be the main risk factor. These results highlight the

256   importance of studying the in-vivo mechanical behaviour of the plantar soft tissues of the MTH area

257   and the clinical relevance of analysing their internal strain fields with the help of medical imaging.

258

259   There are two ways to load the forefoot inside a typical MRI scanner: either by supporting the dorsal

260   side of the passive foot and loading the plantar one [2] or by supporting its plantar side and loading its

261   dorsal one. Considering that pressure is developed at both sides of the foot regardless of the direction

262   of the externally applied load, it becomes clear that the deformations of the dorsal soft tissues will

263   always be unrealistic. Indeed these tissues are not normally meant to be subjected to large

264   compressive loads. On the other hand the plantar soft tissues of the MTH area are compressed

265   between the plantar surface of the loading device and the MTHs. This compressive load within the

266   internal structures will be generated regardless of the direction of the external load either from the

267   dorsal or the plantar aspect of foot. In addition, this scenario closely simulates the loading conditions

268   of quiet stance and the mid-stance phase of gait. The only way to validate the accuracy of this

269   reconstructed internal loading condition is with the help of upright weight bearing MRI, which is

270   beyond the scope of this manuscript.

271

272   In a previous attempt to simulate clinically relevant loading scenarios inside an MRI scanner Petre et

273   al. [2] developed a loading device that was capable of applying "gait-like loading" [2] but couldn't

274   reconstruct subject specific plantar pressure distributions. According to the results presented by Petre

275   et al. [2], the average difference in terms of peak pressure between the reference and the reconstructed

276   loading was 66% while only in 50% of the cases the reconstructed peak pressure was observed under

277   the correct MTH (i.e. the same MTH as in the reference pressure distributions) [2]. This was

278   attributed to the lack of control over the distribution of the load and to the fact that the device applied

279   a net force simultaneously to both the MTH and toe regions [2].

280

281   In order to address this issue the device presented here was equipped with a specially designed punch.

282   This punch is used to compress the forefoot and modify the distribution of the applied load. This

283   unique feature allowed the accurate reconstruction of diverse and distinctive subject specific plantar

284   pressure distribution patterns. Indeed the average difference between the reference and the

285   reconstructed maximum pressures was only 4% and in every case the maximum pressure was

286   observed under the same MTH for both the reconstructed and the reference pressure distributions.

287   Based on these results it can be concluded that the device presented here offers a clear improvement

288   for the reconstruction of subject specific plantar pressure distributions of the MTH area.

289

290   The reproducibility of loading with an accuracy of 5% that was assessed through a test-retest

291   procedure allows the reconstruction of subject specific loading conditions inside an MRI scanner.

292   This allows configuring the device before entering the MRI environment with the use of pressure

293   measurement sensors that are not usually MRI compatible and then to reproduce the same loading

294   conditions inside the scanner.

295

296   Another challenge stems from the fact that MRI scanning can be a rather lengthy process and

297   therefore loading should be kept constant for a significant amount of time. The device presented here

298   was proven capable of keeping loading constant for up to 20 minutes (net force= 150 N, average peak

299   pressure = 111.8 kPa). Even though the results indicated that even higher loads could be sustained for

300   even longer periods of time the actual limits both in terms of loading and time is more likely to be set

301   based on considerations about the comfort and wellbeing of the subject rather than the capabilities of

302   the device. With respect to this, special attention needs to be given to patients with impaired

303   circulation and nerve damage to prevent trauma. Considering the limited access to the device inside

304   the MRI scanner special care should be given to ensure that the toes of the subject are kept in a neutral

305   position and that the skin at the dorsal side of the foot is not over-stretched as a result of loading.

306

307   The second configuration of the device allows the application of bending moments. Even though this

308   loading scenario does not simulate an everyday activity it can give clinically relevant information on

309   foot biomechanics. Imaging the foot under bending loads can shed light on the function of the joints

310   of the foot and the stiffness of their non-contractile tissues, like ligament and tendon stiffness, with

311   implications in assessing the functional impairment in conditions like diabetes.

312

313   In the context of this study the bending stiffness of the MP joints of one subject with no known

314   musculoskeletal abnormality or diabetes was measured for validation and demonstration purposes. As

315   expected, the passive bending stiffness of the MP joints measured here was significantly lower

316   compared to measurements taken during locomotion. Oleson et al.[16] studied the stiffness of the

317   forefoot during running with the use of a motion analysis system. They concluded that the MP joints

318   have a time-depended stiffness and its function resembles that of an "active mechanism" instead of a

319   linear spring [16]. The bending stiffness reported by Oleson et al. [16] was close to 1.6 Nm/deg for a

320   flexion angle of 20 deg while the respective value of the passive stiffness measured here was only

321   0.06 Nm/deg.

322

323   No specific conclusions can be drawn on the mechanical behavior of the MP joints at this point due to

324   the nature and design of this pilot investigation. Although the bending tests were performed on a

325   single subject, further studies will use this device to measure the passive MP joint stiffness of people

326   with no musculoskeletal abnormalities or diabetes as well as of people with diabetes to study

327   differences in terms of joint mobility and stiffness. Previous investigations indicate that people with

328   diabetes are often found to have limited joint mobility which is linked to increased ulceration risk

329   [19]. Increased joint stiffness caused by non-enzymatic glycosylation is presumed to be one of the

330   main contributors of limited joint mobility of the diabetic foot's distal joints [19]. Studying the

331   passive bending stiffness and the mobility of the joints within the diabetic foot will shed light on the

332   causative factors of this pathological change with the potential to help improve current therapeutic

333   approaches for the reduction of ulceration rates.

334

335

336   The type and range of loading scenarios that can be realised using this device is mainly limited by the

337   fact that in its current form it cannot apply combinations of different types of loading such as

338   compression and bending or combined compression and shear. For this reason the plantar pressure

339   reconstructions performed here were limited to load cases where shear loads are minimal such as quiet

340   stance and the mid-stance phase of gait. Despite this limitation the device could be used with minor

341   modifications to study loading scenarios involving compression of the forefoot at different

342   dorsiflexion angles of the toes. The dorsiflexion angle of the toes could be modified easily with the

343   use of wedges with different inclinations. Another limitation of this device is that it cannot be used to

344   study rate dependent phenomena.

345

346   For the purposes of the present study the maximum compressive force applied to a subject was 250 N.

347   Even though this force may seem relatively low compared to the net forces applied to the foot during

348   everyday activities the results of this study indicate that if this force is properly focused it can

349   generate plantar pressures in order of magnitude that are relevant to the cases of quiet stance and mid-

350   stance phase of walking gait. The maximum net compressive force that can be applied by the device

351   is mainly limited by the fact that pressure is applied on a relative small area at the dorsal side of the

352   foot. Because of that increased loads could cause discomfort or trauma. Even though the simulation of

353   loading scenarios involving higher compressive forces at the MTH area (i.e. similar or higher that

354   body weight) were beyond the scope of this study, minor modifications could increase the magnitude

355   of the compressive force that can be safely applied. Increasing the contact area between the

356   compression punch and the dorsal side of the foot would allow the application of significantly higher

357   forces.

358   The MRI compatible loading device presented here can realise clinically relevant loading scenarios

359   and allows the accurate reconstruction of subject specific plantar pressure distributions of the MTH

360   area for the cases of quiet stance and mid-stance phase of gait. The device can be used to validate

361   numerical models of the foot, where the loading is applied by a virtual punch. The validated foot

362   models can then be used to simulate real-life scenarios. In the future this device can be used for the

13

363 investigation of the correlation between plantar pressure and internal tissue stresses and strains as well

364 as for the study of the forefoot's inter-segmental passive stiffness.

365

366 **Acknowledgments**

371

372

373 **Competing interests:** None declared

374

375

376

377

378

379

380

381

382

383

384

385

386

387

388

389

390

391 **References**

392 [1] Yarnitzky G, Yizhar Z, Gefen A. Real-time subject-specific monitoring of internal
393   deformations and stresses in the soft tissues of the foot: A new approach in gait analysis. J
394   Biomech 2006;39:2673–89.

395 [2] Petre MT, Erdemir A, Cavanagh PR. An MRI-compatible foot-loading device for assessment
396   of internal tissue deformation. J Biomech 2008;41:470–4.

397 [3] Gefen A. Plantar soft tissue loading under the medial metatarsals in the standing diabetic foot.
398   Med Eng Phys 2003;25:491–9.

399 [4] Hsu C-C, Tsai W-C, Hsiao T-Y, Tseng F-Y, Shau Y-W, Wang C-L, et al. Diabetic effects on
400   microchambers and macrochambers tissue properties in human heel pads. Clin Biomech
401   (Bristol, Avon) 2009;24:682–6.

402 [5] Gefen A, Megido-Ravid M, Itzchak Y, Arcan M. Biomechanical analysis of the three-
403   dimensional foot structure during gait: a basic tool for clinical applications. J Biomech Eng
404   2000;122:630–9.

405 [6] Gefen A, Megido-Ravid M, Itzchak Y. In vivo biomechanical behavior of the human heel pad
406   during the stance phase of gait. J Biomech 2001;34:1661–5.

407 [7] Smith KE, Commean PK, Mueller MJ, Robertson DD, Pilgram T, Johnson J. Assessment of
408   the diabetic foot using spiral computed tomography imaging and plantar pressure
409   measurements: a technical report. J Rehabil Res Dev 2000;37:31–40.

410 [8] Madsen MT, Haller J, Commean PK, Vannier MW. A device for applying static loads to
411   prosthetic limbs of transtibial amputees during spiral CT examination. J Rehabil Res Dev
412   2000;37:383–7.

413 [9] Commean PK, Mueller MJ, Smith KE, Hastings M, Klaesner J, Pilgram T, et al. Reliability
414   and validity of combined imaging and pressures assessment methods for diabetic feet. Arch
415   Phys Med Rehabil 2002;83:497–505.

416 [10] Petre MT, Erdemir A, Panoskaltsis VP, Spirka TA, Cavanagh PR. Optimization of nonlinear
417   hyperelastic coefficients for foot tissues using a magnetic resonance imaging deformation
418   experiment. J Biomech Eng 2013;135:61001–12.

419 [11] Gefen A. Integration of plantar soft tissue stiffness measurements in routine MRI of the
420   diabetic foot. Clin Biomech 2001;16:921–5.

421 [12] Weaver JB, Doyley M, Cheung Y, Kennedy F, Madsen EL, Van Houten EEW, et al. Imaging
422   the shear modulus of the heel fat pads. Clin Biomech (Bristol, Avon) 2005;20:312–9.

423 [13] Elbannan KM, Salisbury SP. Design of a two degree-of-freedom, MRI-compatible actuator.
424   Conf Proc IEEE Eng Med Biol Soc 2012;2012:940–3.

425 [14] Roy A, Forrester LW, Macko RF, Krebs HI. Passive and active wrist joint stiffness following
426   eccentric exercise. J Rehabil Res Dev 2013;50:555–72.

427 [15] Uppot RN, Sahani D V, Hahn PF, Gervais D, Mueller PR. Impact of obesity on medical
428   imaging and image-guided intervention. AJR Am J Roentgenol 2007;188:433–40.

429 [16] Oleson M, Adler D, Goldsmith P. A comparison of forefoot stiffness in running and running
430   shoe bending stiffness. J Biomech 2005;38:1886–94.

431 [17] Ledoux WR, Shofer JB, Cowley MS, Ahroni JH, Cohen V, Boyko EJ. Diabetic foot ulcer
432   incidence in relation to plantar pressure magnitude and measurement location. J Diabetes
433   Complications 2013;27:621–6.

434 [18] Cavanagh PR, Ulbrecht JS. The biomechancis of the foot in diabetes mellitus. In: Bowker JH,
435   Pfeifer MA, editors. Levin O'Neal's Diabet. Foot, Philadelphia: Elsevier Health Sciences;
436   2008, p. 115–84.

437

438

439

440

441

442

443

444

445

446

447

448

449

450

451

452

453

454

455

456

457 **Tables**

458

459 Table 1: The reference and the reconstructed average peak pressures measured under each MTH for

460 the case of quiet stance (six volunteers) and the respective reference peak pressures and reconstructed

461 average peak pressures (one volunteer) for the case of mid-stance phase of gait. The overall maximum

462 values for each volunteer are highlighted.

		Quiet stance							Mid-stance
Volunteer:		#1	#2	#3	#4	#5 Test	#5 Re-test	#6	#5
Gender (M/F):		F	M	F	M	F	F	F	F
Age (y)		32	35	45	38	30	30	24	30
Weight (Kg):		60	82	72	82	67	67	70	67
1st MTH	Reference/ Reconstructed	29/ 26	176/ 163	46/ 46	69/ 70	218/ 221	218/ 211	50/ 58	57/ 65
2nd MTH	Reference/ Reconstructed	70/ 78	60/ 67	79/ 82	64/ 64	66/ 64	66/ 70	51/ 69	97/ 97
3rd MTH	Reference/ Reconstructed	51/ 52	88/ 90	95/ 91	60/ 57	77/ 42	77/ 46	77/ 76	98/ 106
4th MTH	Reference/ Reconstructed	53/ 53	167/ 151	57/ 80	49/ 50	49/ 40	49/ 42	41/ 35	91/ 85
5th MTH	Reference/ Reconstructed	42/ 41	184/ 185	61/ 62	68/ 66	37/ 35	37/ 38	37/ 38	92/ 81
Mean error (%):		5	6	10	2	15	15	14	8

(Max. Pressure (kPa) labels the rows of MTH measurements.)

463

464

465 Table 2: The results from the pilot testing of the device's bending mode. The bending angle values of

466 all five trials are presented.

Bending moment (Nm)	Bending angle (deg)					Average	STDEV
	Trial 1	Trial 2	Trial 3	Trial 4	Trial 5		
1.8	89	90	90	90	90	90	0
2.2	105	99	103	103	103	103	2
3.3	120	120	119	119	124	120	2
3.9	126	123	127	127	127	126	2
4.6	133	138	139	140	138	138	3

467

468

469   **Figure legends:**

470

471   Figure 1: Two different configurations of the MRI compatible loading device used to apply

472   compressive (A) and bending loads (B). The punch used to apply the compressive load and to control

473   its distribution is also shown.

474

475   Figure 2: MRI images of the forefoot before (A) and after compression (B). The boundaries of the

476   foot and of the visible bones have been manually outlined for both cases (dotted blue and continuous

477   red curves for A and B respectively) and presented together (C) for comparison.

478

479   Figure 3: The reference planar pressures (left) and the ones measured inside the device before (centre)

480   and after (right) the adjustment of the compression punch profile for volunteer #6 (pressure in kPa).

481   The area of the MTHs is defined using a number of polygons. Inside each one of these polygons the

482   location of peak pressure is marked by a rectangle. The average values of the peak pressures of each

483   MTH are also plotted together for comparison.

484

485

486

487

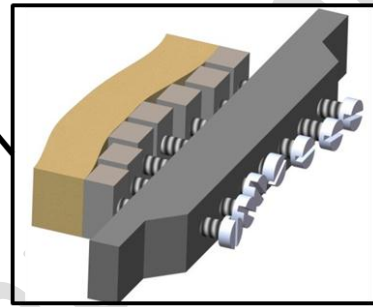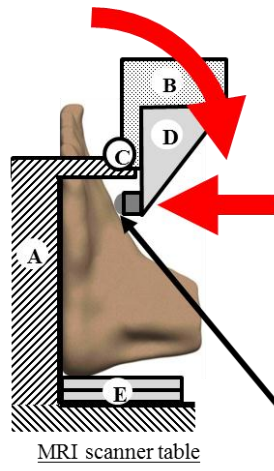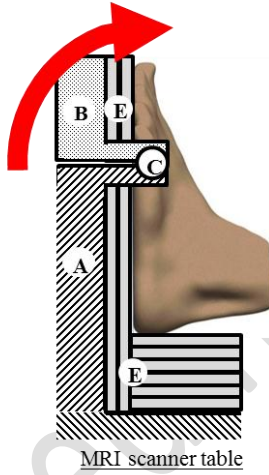488

489

490

491

492

493

494

495

496

497   Figure 1:

498

(A)

MRI scanner table

(B)

MRI scanner table

499

500

501

502

503

504

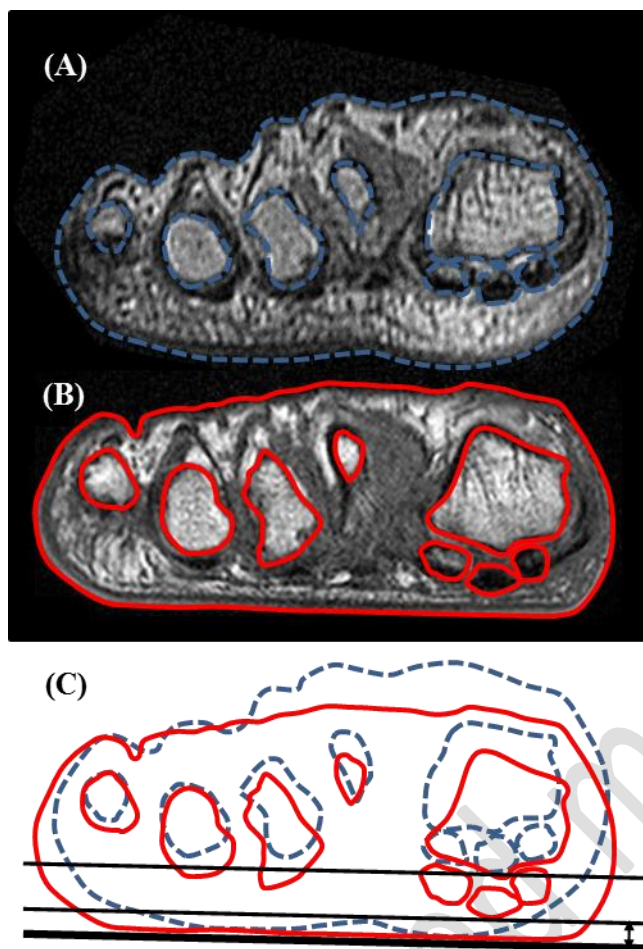505

506

507

508

509

510

511   Figure 2:

512

513
514
515
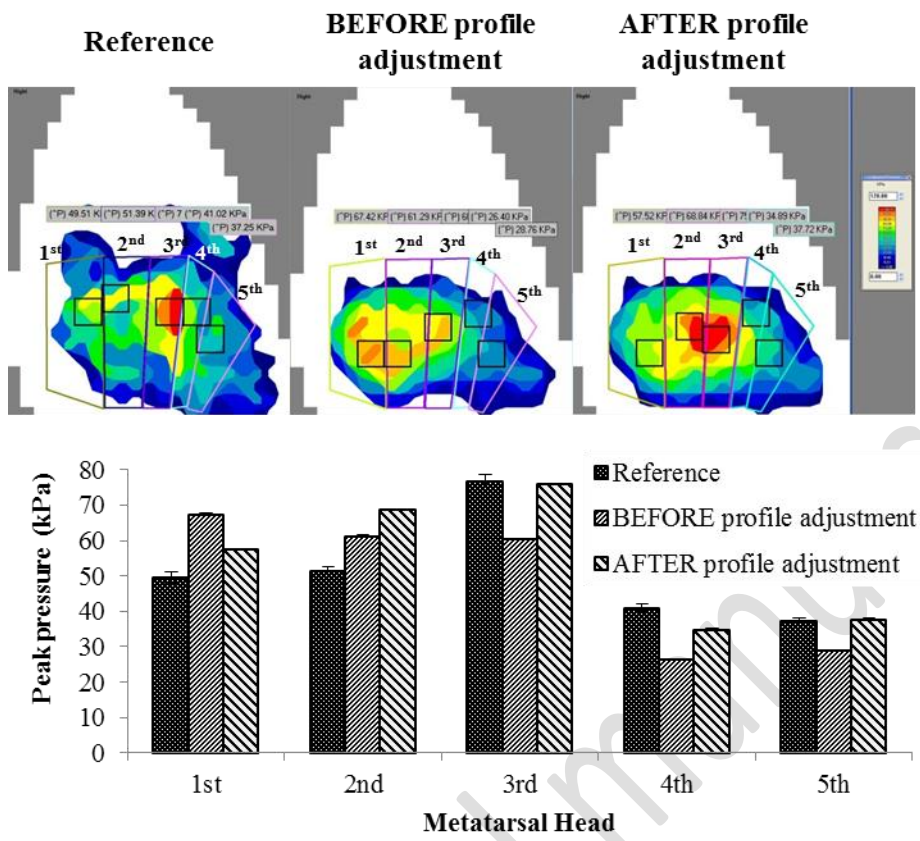516
517
518
519
520
521
522
523
524

525   Figure 3:

526

527
528
529
530
531
532
533
534
535
536
537
538